Acta Crystallographica Section D
Biological Crystallography
ISSN 0907-4449

Effects of PEG on detergent micelles: implications for the crystallization of integral membrane proteins

Carl Hitscherich Jr,[a] Vladimir Aseyev,[a]† John Wiencek[a] and Patrick J. Loll[b]*

[a]Department of Chemical and Biochemical Engineering, University of Iowa, Iowa City, IA 52242, USA, and [b]Department of Pharmacology, University of Pennsylvania, Philadelphia, PA 19104-6084, USA

† Permanent address: Institute of Macromolecular Compounds, Russian Academy of Science, Bolshoi Prospekt 31, 199004 St Petersburg, Russia.

Correspondence e-mail: loll@pharm.med.upenn.edu

Received 24 January 2001
Accepted 11 April 2001

The solubilization of integral membrane proteins with detergents produces protein–detergent complexes (PDCs). Interactions between the detergent moieties of PDCs contribute significantly to their behavior. The effects of the precipitating agent polyethylene glycol (PEG) upon these detergent–detergent interactions have been examined, focusing on the detergent system used to crystallize the bacterial outer membrane protein OmpF porin. Static and dynamic light scattering were used to assess the effects of temperature and concentration upon the hydrodynamic size distribution and the aggregation state of detergent micelles and a phase diagram for micellar solutions was mapped. Estimates of the second osmotic virial coefficient obtained from static light-scattering measurements on micelles were shown to accurately reflect the thermodynamic quality of the solvent. Solvent quality decreases as the consolute boundary is approached, suggesting micelle–micelle attractive forces help to organize PDCs into crystalline aggregates near the cloud point. An apparent increase in micelle mass is observed as the solution approaches the cloud point. These results raise the possibility that the detergent-mediated aggregation of PDCs and/or slight changes in micelle geometry may prove to be important in the nucleation of membrane protein crystals.

1. Introduction

Integral membrane proteins are thought to represent at least 25% of the proteins encoded in the genomes of most organisms (Wallin & von Heijne, 1998). These molecules mediate some of the most important functions carried out by living cells, yet our knowledge of their structure is still rudimentary. This is largely a consequence of obstacles encountered in applying the methods of structural biology to hydrophobic proteins. In particular, X-ray crystallography has been slow to reveal the details of membrane protein structure because of difficulties inherent in the production of large well ordered crystals suitable for diffraction studies.

In order to carry out the biochemical tasks associated with purification and characterization of membrane proteins, it is necessary to solubilize these molecules with detergents. This produces a protein–detergent complex (PDC), wherein the hydrophobic faces of the protein are covered by a micelle-like structure. Once a pure preparation of the PDC has been achieved, two choices are available for the growth of three-dimensional crystals. One method is to reconstitute the protein in a bilayer system such as a cubic lipid phase (Landau & Rosenbusch, 1996; Caffrey, 2000), while the other is to crystallize the PDC directly. The former method has been responsible for several recent successes (Chiu *et al.*, 2000) and

shows great promise; however, as of this writing the majority of membrane protein crystal structures have been derived from crystals grown directly from PDC solutions. Therefore, improved methods for PDC crystallization are a high priority in membrane protein structural biology.

PDCs contain comparable amounts of protein and detergent (le Maire *et al.*, 2000) and the physical characteristics of the PDC reflect the properties of both components. It is therefore not surprising that the detergent moieties play important roles in modulating the crystallization behavior of PDCs. For example, additives known to contribute to the crystallization of particular PDCs appear to achieve their effects by acting upon the physical properties of the detergent species, such as micelle size, number and intermicellar attractive potential (Thiyagarajan & Tiede, 1994). In addition, it is well established that crystallization of PDCs is enhanced under conditions that approach the cloud point of the detergent used (Garavito & Picot, 1990; Rosenbusch, 1990). The cloud point, or consolute boundary, represents a phase boundary at which intermicellar attractive forces become sufficiently strong that micelles coalesce into a separate phase; the correlation between crystallization and detergent cloud point suggests that attractive intermicellar forces between the detergent portions of PDCs play a crucial role in bringing these particles together to sample possible crystal packing arrangements (Zulauf & Rosenbusch, 1983; Zulauf, 1991).

OmpF porin is an outer membrane protein from *Escherichia coli* that was one of the first membrane proteins to be crystallized (Garavito & Rosenbusch, 1986). A variety of different OmpF crystal forms have subsequently been produced and the protein has proven to be useful as a model system for the study of PDC crystallization. Static light scattering (SLS) has revealed that the second osmotic virial coefficient, B_{22}, is a predictor of the crystallization behavior of OmpF PDCs (Hitscherich *et al.*, 2000), as has previously been demonstrated for soluble proteins (George *et al.*, 1997). Perhaps more significantly, under OmpF crystallization conditions the B_{22} behavior of protein-free detergent micelles is very similar to the B_{22} behavior of complete PDCs. This implies that an understanding of micelle–micelle interactions occurring in pure detergent solutions may prove directly relevant to the crystallization of detergent-solubilized membrane proteins (Loll *et al.*, 2001).

A complete understanding of the micelle–micelle interactions that occur during crystallization cannot be achieved using SLS alone. Any changes in micelle size that might occur would confound B_{22} estimates and the radii of gyration of micelles are too small to be measured by SLS. However, size estimates can be obtained from dynamic light scattering (DLS). Hence, to further investigate the contribution of micelle–micelle interactions to PDC crystallization, we have combined SLS and DLS to explore the effects of detergent concentration and temperature on micelle–micelle interactions, micelle size and molar mass. Our studies focused on solutions containing mixed micelles of *n*-octyl-β-D-glucopyranoside (BOG) and *n*-octylpolyoxyethylene (octyl-POE; C_8E_n, n = 2–9) and fixed concentrations of the precipitant PEG. These solutions lie near the detergent cloud point and correspond to conditions known to give rise to OmpF crystals. It is seen that as the cloud point is approached, the detergent micelles interact strongly and form a second population with larger apparent radius. It is possible that such interactions between micellar groups mediate crystal nucleation *via* the formation of PDC aggregates.

2. Experimental

2.1. Materials

Buffer salts were obtained from EM Science and Fisher. Detergents were from Anatrace (BOG) and Bachem (octyl-POE) and PEG 2000 was obtained from Fluka.

The present study focuses on the properties of the mother liquor from which tetragonal crystals of OmpF porin are grown (space group $P4_2$; Garavito & Rosenbusch, 1986). This solution consists of 0.5 *M* NaCl, 0.1 *M* sodium phosphate, 1 m*M* sodium azide, 0.9%(*w*/*w*) BOG and 0.09%(*w*/*w*) octyl-POE pH 6.5; the precipitant used is PEG 2000. Buffers were prepared by titration of 0.1 *M* monobasic and dibasic sodium phosphate solutions containing 0.5 *M* NaCl to yield a pH of 6.5. Sodium azide was added following titration, after which PEG was added to a concentration of 15%(*w*/*w*). Detergent-containing solutions were prepared with a constant weight ratio of octyl-POE to BOG of 1:10. The detergent concentration is defined as the total concentration of both detergents ($c_{\rm det}$) and was varied from 0 to 150 mg ml^{-1}. The micellar concentration (c_m) was assumed to be the total detergent concentration in excess of the critical micelle concentration ($c_m = c_{\rm det} - c_{\rm CMC}$).

All solutions were prepared using distilled deionized water (Maxima, ELGA Inc.) and were filtered using 0.2 µm filters (Puradisc 25TF, Whatman). Filtration was performed at 333–343 K and the integral intensity of scattered light was measured before and after filtration to ensure that no change in detergent and/or PEG concentration took place.

2.2. Instrumentation and methods

2.2.1. Light-scattering measurements. SLS and DLS experiments were conducted with an ALV/SP-125 Compact DLS/SLS goniometer and an ALV-5000/E multiple tau digital correlator. A diode-pumped solid-state laser (COHERENT, DPSS532-400) operating at 532 nm wavelength was used as a light source. SLS measurements were performed at a scattering angle of 90° over the temperature range 278–328 K. Measurement of SLS data from micellar solutions was performed as described in Hitscherich *et al.* (2000). In DLS experiments, the correlation function of the scattered light intensity $G_2(t)$ was measured in the self-beating mode (Chu, 1991) at scattering angles between 30 and 150°. The temperature was varied from 295 to 328 K. Correlation functions were obtained with a shortest sample time of 12.5 ns and a last delay time of 393.2 ns. Time correlation functions were analyzed using the second cumulant fit, the regularized inverse Laplace transform program *CONTIN* and single and double

exponential fits. The specific refractive index (dn/dc) was measured using a Bellingham & Stanley 60/ED Abbe refractometer and the laser light source described above, using the methods detailed in Hitscherich *et al.* (2000). The value obtained for dn/dc was 0.113 ± 0.002 ml g^{-1}; this value was found to be independent of temperature and was consequently used in all SLS calculations.

2.2.2. CMC determination. Static light scattering was used to determine the critical micelle concentration (CMC) for the BOG/octyl-POE detergent system over the temperature range 295–328 K (Shtan'ko *et al.,* 1987; Kameyama & Takagi, 1990; Hitscherich *et al.*, 2000). The CMC was identified by the characteristic sharp break in the plot of Rayleigh ratio *versus* detergent concentration which is indicative of micelle formation. The CMC data are summarized in Table 1.

2.2.3. Cloud-point determination. Detergent cloud points were determined by measuring static light scattering while slowly decreasing the temperature of the solution; estimates were also obtained by visually monitoring solution clouding. The rate of temperature scanning proved critical. If cooling rates were too rapid, estimates of the phase-separation temperature were obtained that were lower than the actual cloud point. If cooling rates were too slow, it was possible to miss the cloud point because phase separation occurred at the top of the sample volume, outside the path of the laser beam. An optimal scanning rate of 6 K h^{-1} was determined by trial and error and was used for all estimates.

2.2.4. Viscosity measurement. The temperature dependence of the viscosity of the 15%(w/w) PEG solution was measured using a Ubbelohde capillary viscometer. Density measurements were conducted at the same temperatures using an Anton PAAR DMA 5000 density meter.

2.3. Theory

2.3.1. Static light scattering. In static light-scattering (SLS) experiments, the time-averaged intensity of scattered light is measured as a function of particle concentration and scattering angle. When extrapolated to zero scattering angle and zero concentration, such measurements yield the weight-averaged molar mass (M_w) and the second osmotic virial coefficient (B_{22}) of the scattering particles. B_{22} is commonly taken as a measure of the pairwise intermolecular forces between particles in solution (Stigter & Hill, 1959).

Because the size of the scattering species (detergent micelles and PEG 2000) is smaller than $\lambda/20$, the excess scattered intensity is independent of scattering angle and the Debye equation applies (Kratochvil, 1987),

$$\frac{Kc}{R_{90}} = \frac{1}{M_w} + 2B_{22}c, \tag{1}$$

where

$$K = \frac{4\pi^2 n_0^2 (\mathrm{d}n/\mathrm{d}c)^2}{N_\mathrm{A}\lambda^4}. \tag{2}$$

c is the concentration of the scattering species in solution, dn/dc is the specific refractive index of the scattering species in the buffer system, N_A is Avogadro's number, λ is the wavelength of the incident laser light source used, n_0 is the refractive index of the solvent buffer system and R_{90} is the excess intensity of scattered light measured from the scattering volume at 90° scattering angle and represented as the Rayleigh ratio.

Table 1
Physical parameters of detergent solutions containing 15%(w/w) PEG obtained at six different temperatures.

Static light scattering measurements were taken at a 90° scattering angle.

Temperature (K)	CMC (mg ml^{-1})	M_w (g mol^{-1})	$B_{22} \times 10^{-4}$ (cm^3 mol g^{-2})
328 ± 0.1	8.2 ± 1.3	7700 ± 330	3.9 ± 0.3
318 ± 0.1	8.5 ± 1.3	10000 ± 310	1.0 ± 0.2
313 ± 0.1	6.7 ± 1.3	9500 ± 500	−0.7 ± 0.1
308 ± 0.1	7.9 ± 1.3	10300 ± 900	−2.4 ± 0.3
303 ± 0.1	8.0 ± 1.3	11200 ± 1000	−4.1 ± 0.6
295 ± 0.1	8.6 ± 1.3	15800 ± 2000	−4.8 ± 1.2

PEG interacts weakly with BOG/octyl-POE micelles and intensities from both scattering species can be treated separately (Thiyagarajan & Tiede, 1994). Thus, M_w and B_{22} of micelles in PEG solutions can be obtained by subtracting the background scattering of detergent-free solutions from that of the micellar solutions. Since the concentration of micelles is given by the detergent concentration in excess of the critical micelle concentration ($c_m = c_\mathrm{det} - c_\mathrm{CMC}$), (1) becomes

$$\frac{Kc_m}{(R_{90} - R_{90,\mathrm{CMC}})} = \frac{1}{M_W} + 2B_{22}c_m, \tag{3}$$

where $R_{90,\mathrm{CMC}}$ is the Rayleigh ratio measured from the detergent solution at the CMC. This allows for the calculation of M_w and B_{22} from light-scattering measurements made as a function of micelle concentration. A typical Debye plot is shown in Fig. 1(*a*) and values of M_w and B_{22} determined using (3) are given in Table 1.

The value of B_{22} is a direct measure of the thermodynamic quality of the solution. Thermodynamic quality is defined as good when solute–solvent interactions are preferred over solute–solute interactions ($B_{22} > 0$) and poor when solute–solute interactions are favored over solute–solvent interactions ($B_{22} < 0$). Good thermodynamic quality implies that the solute (*e.g.* a PDC) is readily soluble in the solvent; poor thermodynamic quality indicates low solubility. As the solution quality changes from good to poor, attractive forces between solutes lead to increased concentration fluctuations, resulting in increased scattered light intensity. Thus, for example, as the cloud point of a detergent solution is approached, a drastic increase in the scattered light intensity (*i.e.* a rapid decrease in solvent quality) signals incipient phase separation. The concept of the thermodynamic quality of the solvent will be utilized in our discussion of the experimental results.

2.3.2. Dynamic light scattering. Dynamic light scattering (DLS) measures fluctuations in the intensity of scattered light which arise from the thermal motion of particles in the system.

Analysis of these temporal fluctuations allows estimation of the diffusion coefficient, D, which can then be used to determine the scattering particle's apparent hydrodynamic radius R_h.

Fluctuations in scattered light intensity are caused by concentration fluctuations of the molecules in the scattering volume. The rate at which the scattered light fluctuates is directly related to how rapidly molecules move in and out of the scattering volume; the time autocorrelation function of the scattered light intensity $G_2(t)$ thus provides a quantitative measure of particle motion. Most theory is developed using the scattered electric field autocorrelation function $g_1(t)$, which is easily calculated from the experimentally measured intensity autocorrelation function by use of the Siegert relationship

$$g_1(t) = \left[\frac{G_2(t) - G_2(\infty)}{G_2(\infty)}\right]^{1/2}, \quad (4)$$

where $G_2(\infty)$ is the baseline of the experimentally measured intensity autocorrelation function.

For non-interacting monodisperse particles that are small compared with the wavelength of light, the scattered field correlation function $g_1(t)$ decays exponentially,

$$g_1(t) \propto \exp(-t/\tau), \quad (5)$$

where τ is the relaxation time of the scattered field correlation function. τ can be related to the diffusion coefficient of the scattering species,

$$\tau = 1/Dq^2. \quad (6)$$

The scattering vector q is given by

$$q = (4\pi n_0/\lambda_0)\sin(\theta/2), \quad (7)$$

where n_0 is the refractive index of the solvent, λ_0 is the wavelength of laser light and θ is the scattering angle. The apparent hydrodynamic radius (R_h) can be determined using the Stokes–Einstein relationship

$$D = \frac{kT}{6\pi\eta_o R_h}, \quad (8)$$

where k is the Boltzmann constant and η_0 is the solvent viscosity at the absolute temperature T.

Information about relaxation time and apparent hydrodynamic radius distributions can be extracted from the data by regressing appropriate theoretical models to the autocorrelation function. If two different sizes of scattering species are expected, a two-exponential fit is performed to estimate the two relaxation times independently,

$$g_1(t) = a_0 + a_1\exp(-t/\tau_1) + a_2\exp(-t/\tau_2), \quad (9)$$

where a_0, a_1 and a_2 are expansion coefficients known as amplitudes and τ_1 and τ_2 are the relaxation times of the field correlation function. Typically, these relaxation times must differ by at least a factor of two in order to obtain statistically significant regression.

Generalizing from this approach to systems having multiple particle sizes or broad size distributions is straightforward in principle, but requires specialized computational approaches in practice. Each scattering species can be represented by a corresponding relaxation time, resulting in a sum of exponentials

$$g_1(t) = a_1\exp(-t/\tau_1) + a_2\exp(-t/\tau_2) + a_3\exp(-t/\tau_3) + \ldots, \quad (10)$$

where the a_n values represent the relative contributions (amplitudes) of each particle size. The *CONTIN* software package (Provencher, 1979) is routinely utilized to perform

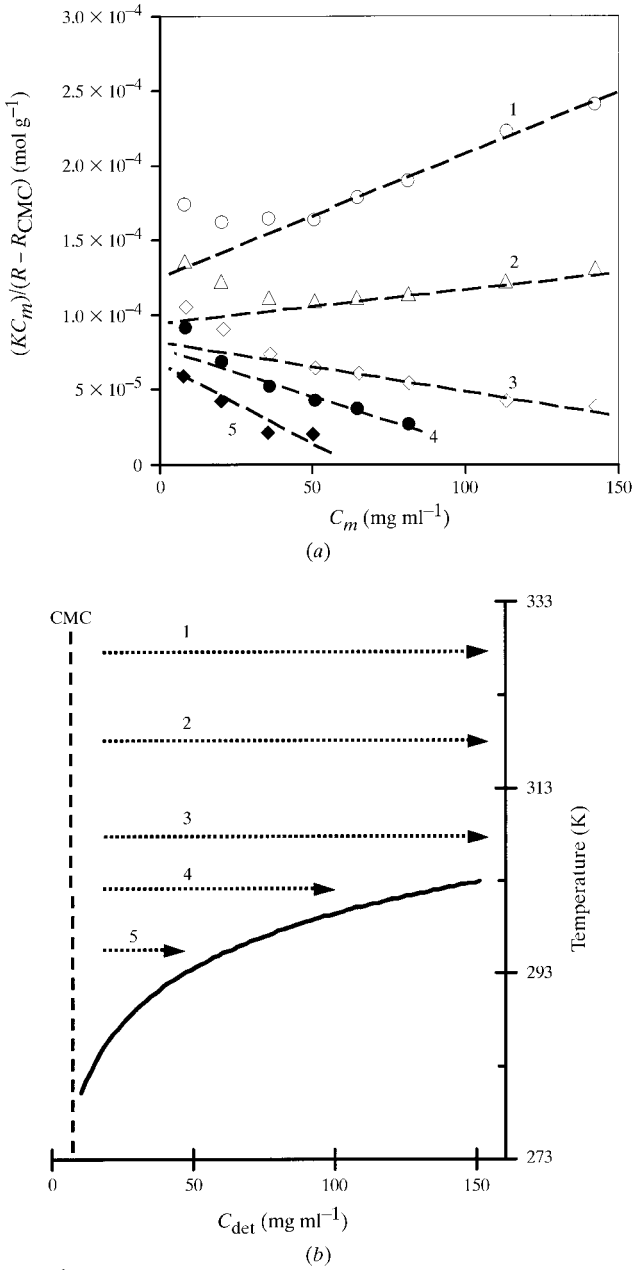

Figure 1
(*a*) Representative Debye plot from mixed BOG/octyl-POE micelles in crystallization buffer containing 15%(*w*/*w*) PEG. The measurements were conducted at the following temperatures: 328 K (1), 318 K (2), 308 K (3), 303 K (4) and 295 K (5). (*b*) Schematic diagram locating the different experimental conditions shown in part (*a*) on a detergent phase diagram; the solid line represents the detergent cloud-point boundary.

such multi-exponential analyses of relaxation-time distributions.

An alternative analysis approach assumes the particle-size distribution to be unimodal. Formally, this approach corresponds to a cumulant expansion of the correlation function (Burchard, 1992) and is usually performed by fitting a third-order polynomial to the field correlation function,

$$\ln[g_1(t)] = \Gamma_0 - \Gamma_1 t + \frac{1}{2!}\Gamma_2 t^2 - \frac{1}{3!}\Gamma_3 t^3. \qquad (11)$$

The polynomial coefficient Γ_1 gives the inverse of the relaxation time ($\tau = 1/\Gamma_1$). Γ_2 is related to the spread of the distribution and is used to calculate the polydispersity index (PDI) of the solution. In cases where multiple species with distinctly different sizes are present, this approach becomes inappropriate.

Once obtained, a relaxation-time distribution may be converted into an apparent hydrodynamic size distribution using the Stokes–Einstein equation. Such size distributions can be unweighted or they can be weighted by the relaxation amplitudes to obtain a mass-weighted radius-distribution function. Mass weighting can be useful because large particles scatter light considerably more efficiently than small particles, which can lead to small quantities of large particles dominating the scattering. For polydisperse samples, the peak value of a mass-weighted distribution is shifted towards smaller sizes in comparison to the unweighted peak value. For monodisperse samples, mass-weighted and unweighted size distributions are the same and cumulant analysis and single exponential fits should yield similar estimates of the mean value of the size distributions.

The true size of a scattering object can be obtained by extrapolating the apparent hydrodynamic radius to infinite dilution. Mazer (1985) discusses the theory underlying the correction of apparent to true hydrodynamic radii and concludes that the correction is insignificant for most micellar systems. This correction requires additional information about thermodynamic parameters, which are not available for the system at hand. For the studies reported in this paper, we have assumed the apparent hydrodynamic radius is essentially equivalent to the true radius. Future publications will address the appropriateness of this assumption.

3. Results and discussion

3.1. Solvent properties

BOG micelles are close in size to the hydrodynamic radius of an individual PEG 2000 molecule (Zhang *et al.*, 1999); this is also expected to be true for the mixed BOG/octyl-POE micelles used in these experiments. Hence, when measuring interactions between these detergent micelles in PEG solutions it is necessary to account for the contribution of PEG to the observed light scattering. To accomplish this, detergent-free PEG solutions were examined by DLS. Fig. 2 depicts the correlation functions of the scattered light intensity obtained from PEG solutions at several scattering angles at 328 K. The correlation functions $G_2(t)$ were normalized using

$$|G_2(t)| = \frac{G_2(t) - G_2(\infty)}{G_2(0) - G_2(\infty)}. \qquad (12)$$

Two relaxation decays of the correlation functions are obvious at scattering angles below 90°. A possible explanation for the existence of two modes is that the 15%(*w*/*w*) PEG solution is semidilute. Single macromolecules are independent and yield unimodal correlation functions in dilute solutions. In more concentrated solutions (intermediate or semidilute solutions), polymer coils interact and even penetrate into each other, forming large aggregates.

To clarify the origin of the slow relaxation process, a dilute solution containing 3%(*w*/*w*) PEG was studied under the same conditions as the concentrated PEG solution. For this solution, the size distributions were found to be unimodal for all scattering angles studied. No angular or temperature dependence of the hydrodynamic size was observed within experimental error. The differences obtained between the unweighted and mass-weighted sizes show that the PEG sample is slightly polydisperse. At 3% PEG, the mean peak value for the unweighted size distribution gave a hydrodynamic radius of $R_h = 1.5$ nm. This value was used to estimate c^*, the lowest PEG concentration at which single PEG coils start overlapping, thus defining the lower limit of the semidilute regime. For a solution of PEG molecules having radius of gyration R_g, c^* can be calculated as for non-interacting hard spheres,

$$c^* = \frac{M_w}{N_A(4\pi/3)R_g^3}. \qquad (13)$$

Since R_g for a single PEG molecule is too small to be measured *via* SLS, its value was estimated as for a monodisperse sample dissolved in a good solvent using $\langle R_g^2 \rangle^{1/2} = 1.78R_h$ (Burchard, 1992), giving $c^* = 4.2\%(w/w)$. Therefore, the solution with 15%(*w*/*w*) PEG concentration can be considered to be semidilute, implying that the PEG molecules overlap. Accordingly, the fast mode of the correlation functions in Fig. 2 corresponds to single PEG molecules

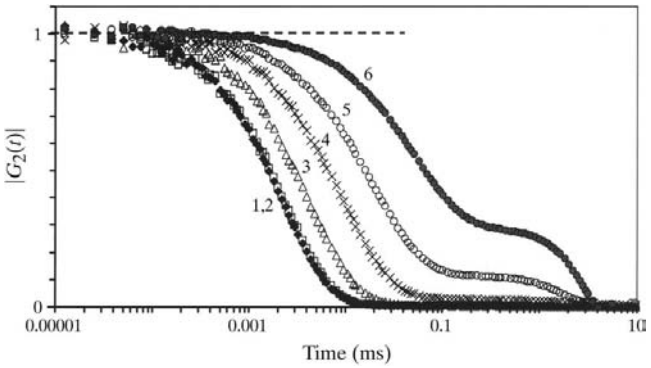

Figure 2
Intensity correlation functions obtained at 328 K at various scattering angles for a solution containing 15%(*w*/*w*) PEG and no detergent. Scattering angle = 150 (1), 135 (2), 90 (3), 60 (4), 45 (5) and 30° (6).

Table 2
Hydrodynamic radii (R_h) calculated for species found in solutions containing 15%(*w*/*w*) PEG and various detergent concentrations, using three different data-analysis methods.

Data obtained at 150° scattering angle and 328 K. R_h values for peak II were calculated using viscosity and refractive index values for a 15%(*w*/*w*) PEG solution, while peak I and second cumulant results were calculated using the viscosity and refractive index of water.

			CONTIN (mean peak value)				Exponential fit	
c_{det}	Second cumulant		Unweighted R_h (nm)		Mass-weighted R_h (nm)		R_h (nm)	
(mg ml^{-1})	R_h (nm)	PDI†	Peak I	Peak II	Peak I	Peak II	Peak I	Peak II
0.0	1.9	0.24	2.0		1.4		2.0	
0.7	1.9	0.22	2.0		1.4		1.9	
6.1	2.0	0.18	2.1		1.5		2.0	
11.2	2.2	0.26	2.4		1.3		2.3	
19.1	3.8	0.40	2.0	2.4	1.8		1.9	2.8
28.5	3.8	0.38	1.9	2.4	1.8		1.7	2.5
58.9	5.5	0.40	1.9	2.6	1.4	1.3	1.9	3.0
73.1	6.1	0.37	2.1	3.0	2.0	2.6	1.9	3.1
89.6	7.3	0.40	2.3	3.6	2.2	3.3	2.1	3.8
104.2	7.2	0.38	2.1	3.6	1.9	2.9	2.2	3.6
121.6	7.6	0.40	2.2	3.8	2.0	2.9	2.1	3.9
150.7	8.2	0.44	2.2	4.4	2.0	3.2	2.1	4.4

† Polydispersity index.

and the slow mode represents formation of short-lived domains (clusters or aggregates) of PEG molecules (Brown, 1993). 3% PEG solutions show only the single-molecule fast mode.

The number and size of the PEG aggregates grow with increasing PEG concentration. As a result, the relative weight of the slow mode increases, which may influence DLS measurements even at a scattering angle of 150°. Thus, the apparent size of PEG molecules ($R_h \simeq 2.0$ nm, see Table 2) measured at 150° for a 15%(*w*/*w*) PEG solution is slightly larger than that ($R_h \simeq 1.5$ nm, see above) measured for the less concentrated 3%(*w*/*w*) PEG solution.

3.2. Properties of micellar solutions

3.2.1. Cloud-point measurements for detergent mixtures. The purpose of this work is to understand the interactions occurring between the detergent moieties of PDCs under crystallization conditions. Since PDCs are known to crystallize preferentially near the cloud point of the detergent used, particular attention must be paid to detergent–detergent interactions near the cloud point and the location of the cloud point must be carefully determined. Aqueous solutions containing BOG as the only detergent are not known to phase separate between 273 and 373 K (Zulauf, 1985, 1991); however, the addition of PEG or salts can induce phase separation in BOG solutions at lower temperatures (Lorber & DeLucas, 1991). When both BOG and octyl-POE are present in solution, mixed micelles are assumed to form. In the presence of PEG, the 10:1 BOG/octyl-POE mixed micelles used in these studies phase separate upon cooling into two immiscible phases, much like pure BOG micelles. The precise location of this cloud-point boundary was mapped using light scattering. Fig. 3 depicts the temperature dependence of the integral of light-scattering intensity observed during a typical cooling scan. The characteristic sharp break in the plot for dilute micellar solutions is well defined and represents the exact cloud point. However, for solutions with higher detergent concentrations, the cloud point is not so clearly defined. Concentration fluctuations increase as the system approaches its critical point; in concentrated solutions, these fluctuations cause opalescence and an increase in the scattered light intensity even at temperatures relatively far from the cloud point. Therefore, for higher detergent concentrations the cloud point was also defined by visually monitoring solution clouding. The results from both types of measurements are shown in Fig. 3.

3.2.2. Static light scattering from micellar systems. Typical SLS results are presented in the Debye plot depicted in Fig. 1(*a*); Fig. 1(*b*) maps these experimental conditions onto the detergent phase diagram. The slope of the Debye plot is proportional to B_{22} and the intercept is equal to the inverse of the scattering-particle molar mass. Molar mass and B_{22} values obtained from such plots are summarized in Table 1. Points on the Debye plot near the CMC deviate from linearity. This occurs because the exact value of the CMC is difficult to define precisely and therefore small errors in

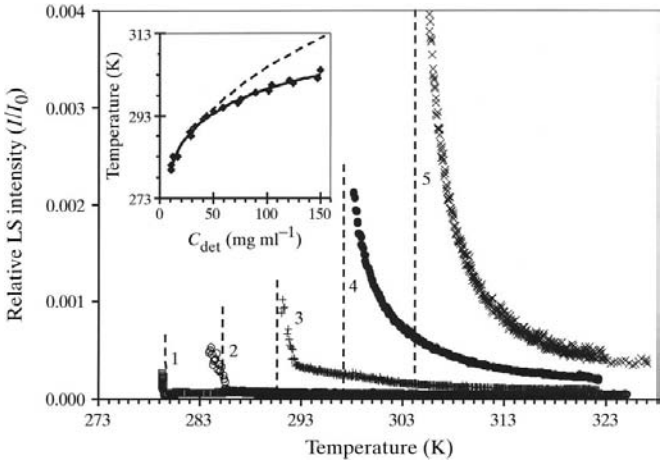

Figure 3
Cloud-point determination by light scattering. The main figure shows the temperature dependence of scattered light intensity obtained at 90° scattering angle for 15%(*w*/*w*) PEG solutions containing various detergent concentrations: 11.2 (1), 16.4 (2), 28.5 (3), 73.1 (4) and 150.7 mg ml^{-1} (5). Light scattering is represented as the ratio of the scattered light intensity to the incident light intensity, I/I_0. Vertical dotted lines show the solution cloud points determined by visual inspection. The inset shows the position of the cloud-point boundary as a function of detergent concentration and temperature; the visually obtained cloud point is shown as a solid line, while the dotted line shows the appearance of critical opalescence as determined by light scattering.

experimentally determined CMC values cause large errors in the calculation of c_m for detergent concentrations near the CMC (Schädler *et al.*, 2000). Hence, points with low c_m values were excluded from M_w and B_{22} calculations.

Upon decreasing temperature (*i.e.* as the cloud point is approached) the measured molar mass of the scattering species increases (Fig. 1). This increase can be a consequence of either increasing mass of the micelles or intermicellar aggregation. Likewise, B_{22} values decrease in magnitude with temperature, signifying that interactions between micelles become more attractive with decreasing temperature. The current SLS results are in good agreement with previous SLS studies conducted on similar buffer systems (Hitscherich *et al.*, 2000); slight differences between the values of B_{22} and molar mass presented here and those obtained previously are most likely to be a consequence of the larger range of detergent concentrations used in the current study.

3.3. Dynamic light scattering

3.3.1. DLS at small scattering angle. To determine whether or not micelle mass changes under different solution conditions, size-distribution studies were conducted on micelles in PEG solutions at different temperatures, varying the detergent concentration from below the CMC to values approaching the cloud point. DLS measurements were carried out at scattering angles of 30 and 150°, in order to distinguish between the contributions of very large particles (which contribute mainly to small-angle scattering) and small particles (for which scattering is independent of angle; Brown, 1993).

Fig. 4 shows the effect of increasing detergent concentration on correlation functions obtained from DLS experiments at a 30° scattering angle and 328 K. The corresponding relaxation-time distributions are also shown in Fig. 4. At detergent concentrations below the CMC, the scattering is principally from PEG; fast and slow modes are observed, corresponding to single PEG molecules and PEG aggregates, respectively. As detergent concentration is increased above the CMC, the relative weight of the slow mode decreases, whereas its relaxation time does not change. This can be understood in terms of the appearance and proliferation of micelles. Micelles are dense and scatter light more efficiently than PEG molecules. Therefore, as the detergent concentration is raised and the number of micelles increases, the micelle scattering swamps the scattering signal generated by PEG molecules. Hence, the slow PEG mode disappears upon increasing detergent concentration even though the solutions remain semidilute with respect to PEG.

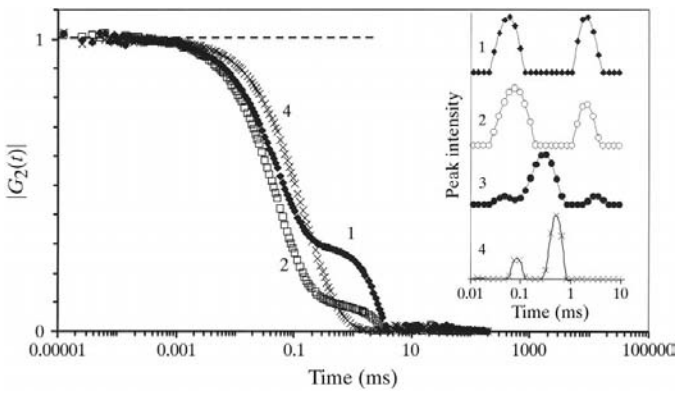

Figure 4
Normalized intensity correlation functions $|G_2(t)|$ and relaxation-time distributions of the field correlation functions $g_1(t)$ obtained at 328 K temperature and 30° scattering angle for aqueous solutions containing 15%(*w*/*w*) PEG and various detergent concentrations: no detergent (1), 11.2 (2), 73.1 (3) and 150.7 mg ml^{-1} (4). For the sake of clarity, the correlation function for the 73.1 mg ml^{-1} concentration is not shown.

The behavior of the fast mode is somewhat more complex. At detergent concentrations below the CMC, the fast mode observed in the relaxation-time distribution corresponds to single PEG molecules. As the detergent concentration is raised to the CMC, this fast-mode peak begins to broaden. This broadening results from the superposition of two peaks, one derived from single PEG molecules and the other from detergent micelles, which are comparable in size to single PEG molecules (Thiyagarajan & Tiede, 1994).

As detergent concentration is further increased, two peaks appear in the fast region of the relaxation-time distribution. There are two possible explanations for this phenomenon. One explanation is that scattering from single PEG molecules becomes insignificant relative to the scattering from detergent micelles and the peak corresponding to single PEG molecules disappears from the distribution. Two separate peaks would then be observed for the detergent species. The position of the faster peak (*i.e.* the peak with the smaller hydrodynamic radius) is independent of detergent concentration; this peak represents detergent micelles. The other fast peak has a size distribution that shifts toward higher hydrodynamic radius as detergent concentration is increased; it corresponds to aggregates of micelles and its relative amplitude grows with increasing detergent concentration. This idea is consistent with the observation of intermicellar aggregates of BOG micelles under similar conditions in SANS experiments (Thiyagarajan & Tiede, 1994).

An alternative explanation is that the fast peak represents only single PEG molecules and the second peak corresponds to single BOG micelles growing in size and/or aggregating with increasing detergent concentration. Further studies aimed at distinguishing between these two possibilities are currently under way.

3.3.2. DLS at large scattering angle. Aggregates of PEG contribute a slow mode to the relaxation-time distribution. The relative amplitude of this mode decreases with increasing scattering angle (Brown, 1993) and it cannot be observed at scattering angles above 90° (Fig. 2). Therefore, to avoid any confounding effects owing to PEG aggregates, a 150° scattering angle was chosen for the analysis of the micellar size distribution. Fig. 6 and Tables 2 and 3 show the results obtained for solutions of various detergent concentrations at different temperatures.

Considerable effort was applied to determining the best strategy for analysis of the correlation functions. A variety of

fitting techniques were tested, including a second cumulant fit and the regularized *CONTIN* program, as well as single and double exponential fits. The appropriate number of exponentials required to fit a correlation function was determined by the relative weight of the two exponential terms (see §2.3.2). A single exponential fit was used until the relative weight of the second exponential (a_2) exceeded 0.1. Particular care was given to a comparison of weighted and unweighted hydrodynamic radius distributions. Numerous trials indicated that the unweighted hydrodynamic radius distributions yielded values of R_h that were most consistent from experiment to experiment. Use of the mass-weighting distribution, in contrast, while providing information about the relative abundance of the different scattering species, proved less useful in the derivation of hydrodynamic radii.

Below the CMC, only single PEG molecules scatter significantly and the apparent hydrodynamic size of this scattering species is independent of detergent concentration (Table 2). At low detergent concentrations, the background solvent is essentially water and so viscosity values measured for water were used in calculating the R_h of the PEG molecules (see equation 8). The unweighted distribution is unimodal with a mean peak value of about 2 nm. All of the analysis methods gave essentially identical results. The difference between the mean R_h values of the mass-weighted and the unweighted distribution arises from the fairly broad relaxation time distribution of the PEG molecules.

Above the CMC, the different analysis methods diverged in their predicted distributions of hydrodynamic radius and it is instructive to consider why this occurs. For example, cumulant analysis fits a single relaxation time and since multiple relaxation times can clearly be identified in the micelle data presented here (Fig. 4), its application is not appropriate. For this reason, the cumulant fit predicts an increase in R_h with increasing detergent concentration (see Table 2). This apparent increase in R_h actually reflects an increase in the size of the higher molecular-weight component (micellar aggregates or growing micelles). The bi-exponential fit and the multi-exponential *CONTIN* fit, on the other hand, yield estimates of hydrodynamic sizes that are in good agreement. A comparison of these two data-analysis methods is presented in Fig. 5, from which it is obvious that above the CMC two relaxation processes exist.

The unweighted size distributions shown in Fig. 6 demonstrate that the position of the slower peak shifts towards larger sizes with increasing detergent concentration. As discussed above, the slower peak corresponds to either intermicellar aggregates or single micelles growing in size. In either case, these particles (intermicellar aggregates or single micelles) are diffusing through the semidilute PEG solution. Therefore, to extract a size distribution from the relaxation-time distribution, the viscosity and index of refraction of the 15%(*w*/*w*) PEG solution must be used for background solvent. The viscosity of this PEG solution was found to be 1.684, 2.084, 2.664 and 3.687 ± 0.005 mPa s at 328, 318, 308 and 295 K, respectively. It was assumed that the faster peak represents PEG molecules and hence all size calculations for this peak were conducted using the viscosity of water. However, this

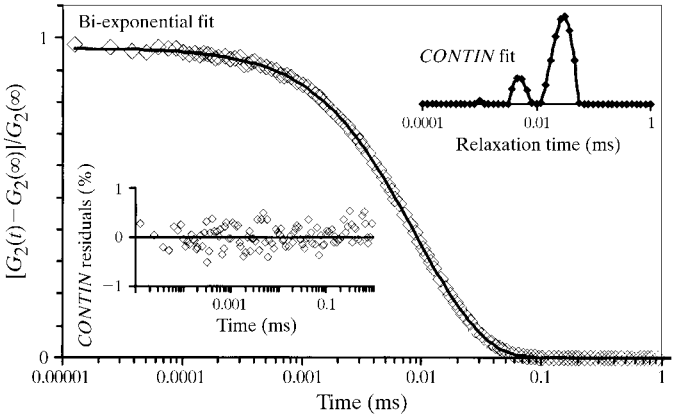

Figure 5
Correlation function data obtained at 328 K and 150° scattering angle from a solution containing 15%(*w*/*w*) PEG and 121.6 mg ml^{-1} detergent. The data were analyzed in two different ways. The upper inset represents a fit obtained with the *CONTIN* program. Two mean peak relaxation times of the $g_1(t)$ correlation function are found: 0.0280 ms (weight = 0.83) and 0.0051 ms (weight = 0.16). The residual errors (expressed as percent deviation from the model fit) are shown in the lower inset; they display no systematic trends, consistent with a good fit. The solid line through the correlation function data represents a bi-exponential fit (equations 4 and 9): $[G_2(t)/G_2(\infty)] - 1 = 3.75 \times 10^{-12} + [0.81\exp(-t/0.0289) + 0.18\exp(-t/0.0050)]^2$. The relaxation times of the corresponding $g_1(t)$ correlation function are 0.0289 ms (weight = 0.81) and 0.0050 ms (weight = 0.18), in good agreement with the *CONTIN* results.

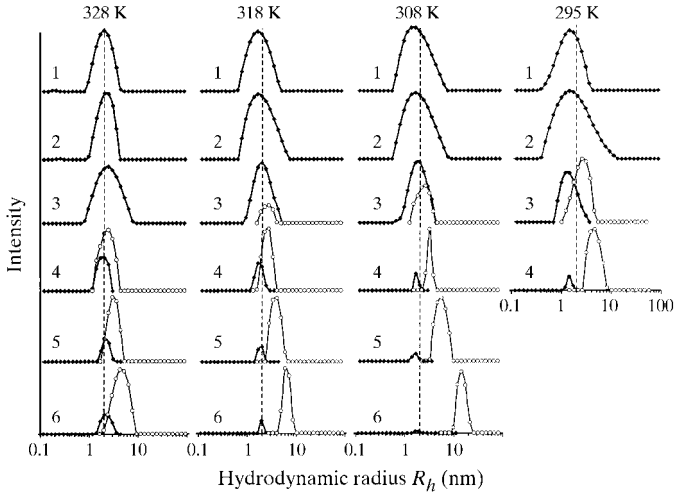

Figure 6
Unweighted hydrodynamic size distributions obtained at 150° scattering angle and four temperatures for 15%(*w*/*w*) PEG aqueous solutions containing various detergent concentrations: no detergent (1), 6.1 (2), 11.2 (3), 28.5 (4), 73.1 (5) and 150.7 mg ml^{-1} (6). Data were analyzed using *CONTIN*. Samples with detergent concentrations in excess of 70 mg ml^{-1} cloud at 295 K and therefore do not appear in the figure. Open dots represent size distributions calculated using the PEG solution viscosity; closed dots, size distributions calculated using water viscosity. Dotted vertical lines show the position in the size distribution of the PEG monomer peak at 328 K.

Table 3
Hydrodynamic radii obtained from unweighted size distributions, calculated with *CONTIN*.

Solutions contained 15%(*w*/*w*) PEG and various detergent concentrations; data were obtained at 150° scattering angle.

	Hydrodynamic radius R_h (nm)							
	328 K		318 K		308 K		295 K	
c_{det} (mg ml^{-1})	Peak I	Peak II	Peak I	Peak II	Peak I	Peak II	Peak I	Peak II
0.0	2.0		1.7		1.7		1.4	
0.7	2.0		1.7		1.8		1.5	
1.5	2.0		1.7		1.5		1.5	
3.4	2.0		1.8		1.7		1.5	
6.1	2.1		1.9		1.8		1.7	
11.2	2.4		2.0	2.8	1.6	2.6	1.4	2.6
19.1	2.0	2.4	1.9	2.5	1.6	3.0	1.4	4.4
28.5	1.9	2.4	1.7	2.5	1.7	3.1	1.5	4.6
58.9	1.9	2.6	1.9	3.6	1.6	4.7	1.6	9.8
73.1	2.1	3.0	1.8	3.8	1.6	5.4	—	—
89.6	2.3	3.6	1.9	4.5	1.8	6.8	—	—
104.2	2.1	3.6	1.9	4.8	1.6	8.1	—	—
121.6	2.2	3.8	1.8	5.5	1.6	10.4	—	—
150.7	2.2	4.4	2.0	6.5	1.7	14.7	—	—

may not be entirely correct, since above the CMC this peak may reflect contributions from both PEG single molecules and from BOG micelles. The contribution of BOG micelles to the faster peak is currently under investigation and will be addressed in future publications.

At the CMC, the polydispersity index (PDI) increases drastically, indicating a broadening of the size distribution. At the same time, micellar scattering begins to overwhelm the scattering of individual PEG molecules. The broad distribution eventually resolves into two separate peaks in the relaxation-time distribution (Fig. 6). The fast peak (lower R_h) corresponds to PEG molecules, with a possible contribution from detergent micelles. The R_h value for this peak is independent of detergent concentration, indicating that if there is a significant micellar contribution, this population of micelles does not increase in mass as the cloud point is approached. The slow peak (high R_h) corresponds to aggregates of micelles or growing micelles. The relative contribution of the aggregate peak becomes more pronounced as detergent concentration is increased; in addition, the hydrodynamic radius of these aggregates increases steadily with increasing detergent.

The distribution of relaxation times was also studied at scattering angles of 135, 90, 60 and 45°. No angular dependence of the hydrodynamic radius was observed for either micelles or micellar aggregates. This finding allows one to assume that the shape of the detergent micelles is approximately isotropic, with a fairly narrow size distribution. The hydrodynamic radius of mixed micelles measured at 328 K was found to be about 2.1 nm, decreasing to a value of about 1.5 nm at 295 K, in good agreement with results obtained using small-angle neutron and X-ray scattering (Table 3; Thiyagarajan & Tiede, 1994; Zhang *et al.*, 1999). In contrast, the radius of the micellar aggregates was found to grow with increasing detergent concentration. As the cloud point is approached, the size of these aggregates can become quite large. Assuming the aggregates contain randomly close-packed spherical micelles with radius R_h leads to an estimate of ∼500 micelles per aggregate. Since the aggregates are unlikely to be so densely packed, this number is probably an overestimate; however, it is clear that the micellar aggregates are capable of becoming quite large near the consolute boundary.

3.4. Interpretation of combined SLS/DLS results: implications for PDC crystallization

The long-term goal of this work is a detailed understanding of the contributions of inter-micellar attractive forces to the association and crystallization of PDCs. Toward this end, SLS was used to measure B_{22}, which is an indicator of the attractive forces between micelles under crystallization conditions (Hitscherich *et al.*, 2000). The SLS results suggest that precipitant drives the system toward crystallization by modulating the micelle–micelle B_{22} value, moving it into the crystallization slot (George *et al.*, 1997). However, the SLS data also suggest that micelles grow in size with increasing detergent concentration. To assist in evaluating the relative contributions of these effects, micelle size was measured. This was accomplished *via* DLS, since the micelles under study are too small for size analysis using SLS. Fig. 6 and Table 3 map the dependence of the unweighted size distribution upon temperature. It is clear that micelles undergo changes upon approaching the cloud point, corresponding to growth and/or aggregation, consistent with the apparent increase in micelle M_w that is observed with decreasing temperature in SLS experiments (Fig. 1).

Taken in conjunction, the results of the SLS and DLS experiments suggest a model to describe the crystallization of PDCs. As the detergent cloud point is approached (by increasing precipitant concentration and/or by manipulating temperature), the thermodynamic quality of the solvent for micelles changes from good to poor (as reflected by the decrease in B_{22} values) and micelle–micelle interactions become progressively more favored over micelle–solvent interactions. The observed correlation between PDC crystallization and detergent cloud point can be explained by the fact that for micelles and PDCs the zone of optimal B_{22} values lies near the cloud point. This zone corresponds to the crystallization slot (George *et al.*, 1997), *i.e.* a region where slightly attractive interparticle forces dominate, providing conditions that promote the association of PDCs and their assembly into crystalline aggregates without encouraging non-specific aggregation. This model is likely to be fairly general for membrane-protein crystal growth (since many different membrane proteins crystallize near the detergent cloud point);

however, in cases where crystals are formed by a 'salting-in' mechanism (*e.g.* Klukas *et al.*, 1999), detergent–detergent interactions may play a less significant role.

The role of micellar aggregates or growing micelles in crystal growth remains unclear. One possibility is that aggregates are required for the formation of crystal nuclei; a related possibility is that micelle growth is required before nucleation can occur. For example, it was once thought that a cloud-point phase separation might actually be required in order for crystals to form: after phase separation occurred, PDCs would partition into the detergent-rich phase, producing a system with high local PDC concentrations that promoted crystal nucleation (Garavito & Rosenbusch, 1980). Subsequent work has shown that crossing the cloud-point boundary is in most cases deleterious to crystal quality; however, partitioning of PDCs into micellar aggregates or enlarged micelles near the cloud point may promote nucleation by a similar mechanism. Once nuclei are formed, their growth would be favored by the slightly attractive micelle–micelle forces found under these conditions, which would encourage the recruitment of PDC monomers to the growing crystal.

An alternate possibility is that aggregates do not lie on the crystallization pathway and are not required for crystal nucleation or growth; *i.e.* their formation under crystallization conditions is coincidental. In this case, the only important process underlying crystal lattice formation would be the pairwise association of monomeric PDCs driven by attractive micelle–micelle forces. These forces would be sufficient to bring PDCs into close proximity so that nucleation could occur by formation of specific contacts between the solvent-exposed protein moieties of the particles.

Studies of PDC crystallization systems other than OmpF may allow discrimination between these two possibilities by determining whether or not micellar aggregate formation or growth are invariably associated with conditions that promote PDC crystallization.

This work was supported by a grant to PJL and JW from NASA (NAG8-1350). The authors are grateful to Professor E. Geissler for assistance in interpretating experimental results and for useful comments.

References

Brown, W. (1993). *Dynamic Light Scattering: The Method and Some Applications.* Oxford: Clarendon Press.
Burchard, W. (1992). In *Laser Light Scattering in Biochemistry*, edited by S. E. Harding, D. B. Sattelle & V. A. Bloomfield. Cambridge: Royal Society of Chemistry.
Caffrey, M. (2000). *Curr. Opin. Struct. Biol.* **10**, 486–497.
Chiu, M. L., Nollert, P., Loewen, M. C., Belrhali, H., Pebay-Peyroula, E. & Rosenbusch, J. P. (2000). *Acta Cryst.* D**56**, 781–784.
Chu, B. (1991). *Laser Light Scattering: Basic Principles and Practice*, 2nd ed., p. 74. San Diego: Academic Press.
Garavito, R. M. & Picot, D. (1990). *Methods*, **1**, 57–69.
Garavito, R. M. & Rosenbusch, J. P. (1980). *J. Cell Biol.* **86**, 327–329.
Garavito, R. M. & Rosenbusch, J. P. (1986). *Methods Enzymol.* **125**, 309–328.
George, A., Chiang, Y., Guo, B., Arabshahi, A., Cai, Z. & Wilson, W. W. (1997). *Methods Enzymol.* **276**, 100–110.
Hitscherich, C., Kaplan, J., Allaman, M., Wiencek, J. & Loll, P. J. (2000). *Protein Sci.* **9**, 1559–1566.
Kameyama, K. & Takagi, T. (1990). *J. Colloid Interf. Sci.* **137**, 1–10.
Klukas, O., Schubert, W. D., Jordan, P., Krauss, N., Fromme, P., Witt, H. T. & Saenger, W. (1999). *J. Biol. Chem.* **274**, 7351–7360.
Kratochvil, P. (1987). *Classical Light Scattering From Polymer Solutions.* Amsterdam: Elsevier.
Landau, E. M. & Rosenbusch, J. P. (1996). *Proc. Natl Acad. Sci. USA*, **93**, 14532–14535.
Loll, P. J., Allaman, M. & Wiencek, J. (2001). In the press.
Lorber, B. & DeLucas, L. J. (1991). *J. Cryst. Growth*, **110**, 103–113.
Maire, M. le, Champeil, P. & Moller, J. V. (2000). *Biochim. Biophys. Acta*, **1508**, 86–111.
Mazer, N. A. (1985). *Dynamic Light Scattering: Applications of Photon Correlation Spectroscopy*, edited by R. Pecora, pp. 305–346. New York: Plenum Press.
Provencher, S. W. (1979). *Makromol. Chem.* **180**, 201–209.
Rosenbusch, J. P. (1990). *J. Struct. Biol.* **104**, 134–138.
Schädler, V., Nardin, C., Wiesner, U. & Mendes, E. (2000). *J. Phys. Chem. B*, **104**, 5049–5052.
Shtan'ko, S. P., Volkov, V. A. & Shakhparanov, M. I. (1987). *Russ. J. Phys. Chem.* **61**, 1470–1471.
Stigter, D. & Hill, T. L. (1959). *J. Phys. Chem.* **63**, 551–556.
Thiyagarajan, P. & Tiede, D. M. (1994). *J. Phys. Chem.* **98**, 10343–10351.
Wallin, E. & von Heijne, G. (1998). *Protein Sci.* **7**, 1029–1038.
Zhang, R., Marone, P. A., Thiyagarajan, P. & Tiede, D. M. (1999). *Langmuir*, **15**, 7510–7519.
Zulauf, M. (1985). *Physics of Amphiphiles: Micelles, Vesicles and Macromolecules*, edited by V. Degiorgio & M. Corti, pp. 663–673. Amsterdam: Elsevier.
Zulauf, M. (1991). *Crystallization of Membrane Proteins*, edited by H. Michel, pp. 53–72. Boca Raton, FL, USA: CRC Press.
Zulauf, M. & Rosenbusch, J. P. (1983). *J. Phys. Chem.* **87**, 856–862.